

Global ERS 1 and 2 and NSCAT observations: Upwind/crosswind and upwind/downwind measurements

Y. Quilfen, B. Chapron, A. Bentamy, and J. Gourrion

Département d'Océanographie Spatiale, IFREMER, Plouzané, France

T. El Fouhaily and D. Vandemark

NASA Goddard Space Flight Center, Wallops Flight Facility, Laboratory for Hydrospheric Processes, Wallops Island, Virginia

Abstract. This paper presents an analysis of the wind speed dependence of upwind/downwind asymmetry (UDA) and upwind-crosswind anisotropy (UCA) as derived from global C band VV-polarized ERS 1 and 2 and Ku band VV- and HH-polarized NASA scatterometer (NSCAT) data. Interpretation of the results relies on identifying relationships between the differing frequencies and incidence angles that are consistent with Bragg scattering theory from gravity-capillary waves. It is shown that globally derived parameters characterizing UDA and UCA hold information on the wind dependence of short gravity and gravity-capillary wave growth and dissipation. In particular, the UCA behavior is found quadratic for both the C and Ku band, peaking at moderate wind speeds. In addition, the dual-frequency results appear to map out the expected, more rapid adjustment of centimeter-scale (Ku band) waves to the wind direction at light winds. However, as wind increases, the directionality associated with these shorter waves saturates at a lower speed than for the slightly longer waves inferred at C band. It is suggested that this observed phenomenon may be related to increasing wave-drift interactions that can potentially inhibit short-scale surface wave growth along the wind direction. Concerning UDA properties, our present analysis reveals that the NSCAT and ERS 1 and 2 scatterometers give quite different results. Our preliminary interpretation is that C band measurements may be easier to interpret using composite Bragg scattering theory and that upwind/downwind contrasts are mainly supported by short gravity waves.

1. Introduction

One robust indicator that the ocean surface exhibits non-Gaussian characteristics and directional anisotropy is the ocean scatterometer's dependable measurement of higher radar backscatter from the upwind look direction when compared to the downwind and the crosswind. An ad hoc accounting for these phenomena is included in data-derived scatterometer wind speed models [Schroeder *et al.*, 1982; Freilich and Dunbar, 1993; Stoffelen and Anderson, 1997]. Typically, two terms, an odd and an even, are introduced in a three-term Fourier model for the ocean's normalized radar cross section (NRCS) versus azimuth viewing angle with respect to wind direction, written as

$$\sigma_0(U, \theta, \phi) = a_0(U, \theta) + a_1(U, \theta) \cos(\phi) + a_2(U, \theta) \cos(2\phi) \quad (1)$$

where U is the near-surface wind speed, θ is the radar's incidence angle, and ϕ is the wind direction relative to the radar's azimuth look direction. In (1) the first-order coefficient a_1 term provides the scaling for what is frequently referred to as an upwind-downwind asymmetry (UDA), the second-order term a_2 scales the upwind-crosswind anisotropy (UCA).

The main task of satellite scatterometers such as ESA's ERS

1 and 2 and NASA's NSCAT is to provide global wind vector information. This is done using primarily the even-order harmonics of (1) because UDA is a small component of σ_0 measurements, especially for vertically polarized instruments, thus leaving a 180° direction ambiguity. The Numerical Weather Prediction (NWP) numerical model winds are used to remove this ambiguity in the operational ERS and NSCAT products. While the UDA measurement is not too critical to current wind vector retrievals, this does not eliminate the need to understand or utilize this information. The fact that UDA is a fundamental component of scatterometer and synthetic aperture radar (SAR) measurements suggests the potential for gaining further insight on wind-wave coupling and microwave scattering and emission from the ocean.

Furthermore, in this decade, ERS 1, ERS 2, NSCAT, and future QuikSCAT satellite measurements are providing global estimates of wind vector and radar cross section on a daily basis. These large data sets permit robust determination of the global characteristics of UDA and UCA versus varying wind speed and other possible correlatives. Proper interpretation and use of UDA and UCA data may give new insight into scatterometer sensor science to help wind vector retrieval development, as well as to possibly characterize geographical differences in the dynamical ocean surface (wind and wave coupling) behavior around the globe.

This paper presents analysis of the wind speed dependence of both UDA and UCA as derived from C band VV-polarized ERS 1 and 2 and Ku band VV- and HH-polarized NSCAT

Copyright 1999 by the American Geophysical Union.

Paper number 1998JC900113.
0148-0227/99/1998JC900113\$09.00

scatterometer data. Background is provided in section 2 on relevant aspects of physical modeling related to both upwind/crosswind and upwind/downwind differences. Analysis is focused on the higher incidence angles $\geq 30^\circ$. In section 3 we first describe how UCA and UDA are derived from the radar cross-section measurements. To generate these observations, we utilize collocation of radar cross section measurements from ERS and NSCAT with the European Centre for Medium-Range Weather Forecasts (ECMWF) model surface wind analysis. For certainty we also compare these estimates with the empirical backscattering model predictions. Interpretation of the results is then presented, relying on relationships between the differing frequencies and incidence angles that are consistent with Bragg scattering from gravity-capillary waves for UCA and the skewness of the slope probability density function (pdf) for UDA.

2. Background

Numerous investigators have proposed theoretical models for UDA and UCA observations. However, the mechanisms of interaction between wind-roughened sea surfaces and these radar signatures are far from being fully understood, and to date, the most successful scatterometer functions are empirically derived.

When trying to determine a physically based scattering model for the ocean surface, two sets of approximations are currently used. The first set of approximations concerns the scattering theory (e.g., the correlation method or the small perturbation method). The second set enters in the statistical description used to ensemble average the predicted cross section. For the range of incidence angle used in scatterometry, 20° – 60° , the return is assumed to be mainly determined by the strength of the surface vertical displacement of small-scale ripples riding over longer waves, i.e., the composite surface Bragg mechanism. The effect of the large scale on Bragg scattering is to tilt and modulate the Bragg scatterers. Indeed, the normal to a slightly rough patch will deviate from the vertical for both parallel and perpendicular incidence planes. The average cross section is then obtained from an average over all possible tilts. Since the centrosymmetric nature of a spectrum does not permit discrimination between upwind and downwind directions, it is necessary to include a modulation of short Bragg-resonant waves to physically model UDA. Presently, there are two main schools of thought on how to reproduce UDA in electromagnetic scattering models.

The first approach employs the modulation transfer function (MTF) concept [e.g., *Plant*, 1986]. It is the combined effect of longwave tilt and shortwave modulation that directly contributes to a_1 ; pure tilt and hydrodynamic modulations contribute to a_0 and a_2 . Moreover, differences between HH and VV polarization modeled radar cross sections may be better explained from such a composite model than from a pure tilt model [i.e., *Romeiser and Alpers*, 1997]. While the concept would appear to be attractive, there is much spread in measured and predicted MTFs. In particular, variations of wind stress along the surface are of crucial influence but are difficult to predict theoretically.

The second approach is to directly consider a non-Gaussian sea surface statistical description [e.g., *Fung*, 1994]. Following this development, hydrodynamic effects on ocean surface are directly introduced using the lowest-order correction to the Gaussian approximation, the bispectrum function, along with

the standard second-order surface spectrum. For wind-roughened sea surface the bispectrum function is difficult to define experimentally. However, in practice, recent applications showed that an ad hoc empirical bispectrum function definition can readily reproduce a given UDA observation [*Chen et al.*, 1992, 1993]. To date, a physical basis has not been given to support the formulation, and therefore one is left with yet another empirical adjustment that makes direct comparisons to other models and data sets difficult.

Models for the UCA observation are generally most dependent on the directional spreading function of the proposed sea wave spectrum. Yet the resulting formulations can be quite different. However, according to recently developed spectral spreading models [cf. *Caudal and Hauser*, 1996; *Elfouhaily et al.*, 1997], there is consensus that the shorter waves tend to be increasingly aligned with the mean wind direction. Such an increase of azimuthal anisotropy in the high-wavenumber region is in accordance with conclusions that can be drawn from sea surface slope measurements as given by *Cox and Munk* [1954] and subsequently analyzed by *Wu* [1990]. Note that slope skewness measurements, as reported by *Cox and Munk*, must also be associated with short-scale surface waves. Indeed, *Cox and Munk's* Sun glitter reflection measurements clearly show that under slick surface conditions, where short-scale surface waves were eliminated, both slope skewness and azimuthal anisotropy were effectively strongly reduced. At a minimum this indicates the necessary presence of small ripples to generate UDA and UCA.

Hereafter, we propose to explore the information that can be gained in the small wave spectral range, by exploiting the combined results from ERS 1, ERS 2, and NSCAT scatterometers. As a function of incidence angle, the C band observations are expected to give information associated with a range of short gravity waves from 10 to 3 cm, while the Ku band observations cover the capillarity-gravity range from 3 to 1 cm; these shorter waves are expected to come more quickly in equilibrium with the wind.

3. Exploration of Global Scatterometer Data and Model Comparisons

We present results obtained from comparisons between ERS 1, ERS 2, and NSCAT off-line products and surface parameters derived from the ECMWF model wind analysis. The NSCAT products used in this paper correspond to the reprocessed data provided by the *Jet Propulsion Laboratory (JPL)* [1997]. NSCAT data collected from May 14, 1997, to June 25, 1997, are used. The surface quality flags within the NSCAT level 1.7 products are used to check the quality of the backscatter coefficients. Conservative use of quality flags insures ocean backscatter coefficients are free from atmospheric, sea ice, or sensor calibration effects. The ERS 1 and 2 products used in this paper correspond to the reprocessed data provided by Institut Français de Recherche pour l'Exploitation de la Mer (IFREMER) [*Quilfen and Bentamy*, 1994]. Thirty weeks of ERS 1 and 2 data were collected covering the years 1992 to 1997 and sampling the summer and winter seasons. The surface quality flags are used to ensure the quality of the backscatter coefficients. We have used less NSCAT data because only these 7 weeks of reprocessed NSCAT data were available at the time we performed the analysis (corresponding to 14 weeks of ERS data in term of data coverage). However, as shown in the following section, this is sufficient to reproduce

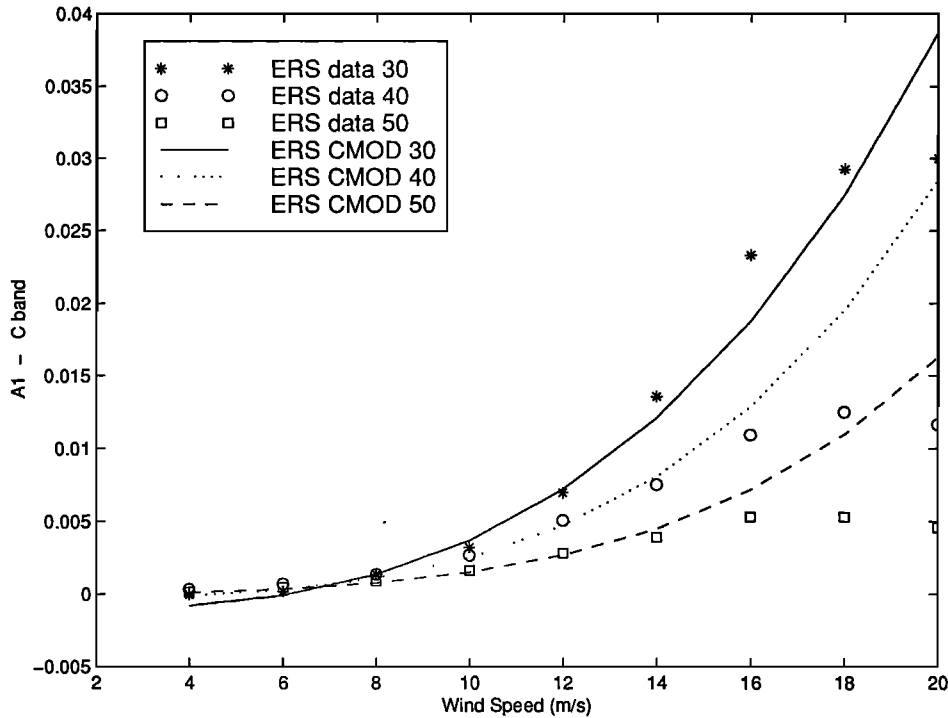


Figure 1. Estimates of coefficient a_1 at C band as computed from the measurements (symbols) and as derived from the CMOD-IFR2 model (lines) as a function of wind speed for three different incidence angles.

well the Ku band empirical backscattering model behavior and thus does not affect significantly the results.

In the following section, we examine the behavior of C band VV polarization ERS data and Ku band VV and HH polarization NSCAT data according to incidence angle, wind speed, and direction. We perform evaluation of the satellite scatterometer backscatter coefficients as a function of independent model analyzed wind fields. Two 6-hour ECMWF outputs are linearly interpolated in space and time to scatterometer points. Collocation with ECMWF winds is done for all NSCAT and ERS observations over the global ocean, up to 60° of latitude.

The a_0 , a_1 , and a_2 Fourier coefficients in (1) are estimated as a function of both incidence angle and wind speed in 1° and 1 m s⁻¹ bins, respectively, as follows:

$$a_0 = (\sigma_{0u} + \sigma_{0d} + 2\sigma_{0c})/4 \quad (2)$$

$$a_1 = (\sigma_{0u} - \sigma_{0d})/2 \quad (3)$$

$$a_2 = a_0 - \sigma_{0c} \quad (4)$$

where σ_{0u} , σ_{0d} , and σ_{0c} are the upwind, downwind, and crosswind σ_0 estimates, respectively. To obtain a_0 , a_1 , and a_2 in one bin, we first collect all the upwind, downwind, and crosswind σ_0 measurements in 20° wide sectors relative to the wind direction/beam azimuth (the ECMWF wind direction is considered as reference). We then compute as many a_0 , a_1 , and a_2 estimates using (2), (3), and (4) as $(\sigma_{0u}, \sigma_{0d}, \sigma_{0c})$ triplets (each measurement is only used once) and average them. The a_0 , a_1 , and a_2 coefficients whose values exceed the median value by plus or minus 3 standard deviations are discarded before estimating the mean values in each bin. The mean values are computed when at least 10 estimates of the Fourier coefficients are available in each bin. The number of collocated data in a bin will thus vary from a minimum of 10 for the

highest winds to a few hundred for milder winds. The averaging of a_0 , a_1 , and a_2 is performed in linear space. Different analysis techniques may affect the Fourier coefficient estimates. One is the data sampling over 20° wide sectors relative to the wind direction/beam azimuth; this is supposed to have little effect on the coefficient estimation because they are smooth functions of the wind direction. More crucial could be the effect of random errors in the ECMWF reference wind speed used for data binning. Indeed, as demonstrated by *Stofelen* [1998], the representativeness errors of the reference wind induce pseudobiases when comparisons are made without taking into account these errors. To overcome this difficulty without having to precisely model the wind errors, we also computed the a_0 , a_1 , and a_2 estimates by using the scatterometer-derived wind speed as a reference for the binning process (NSCAT winds to compute ERS Fourier coefficients and ERS winds to compute NSCAT Fourier coefficients). For clarity purposes the results presented hereafter have only been obtained with the ECMWF winds, but conclusions on the certainty of observed biases are drawn only when they are evidenced in both computations.

3.1. UDA Analysis

Figure 1 shows a_1 parameters obtained from ERS C band measurements and CMOD-IFR2 empirical model predictions [Quilfen *et al.*, 1998]. As defined following equation (1), a_1 coefficients are increasing with wind speed up to about 15 m s⁻¹ and decreasing for the incidence angles considered. For the highest wind speeds, observed a_1 parameters tend to saturate and/or to decrease. This is not well captured by the model.

As it has been pointed out by *Bentamy et al.* [1994] in their calibration efforts, their use of a polynomial decomposition for

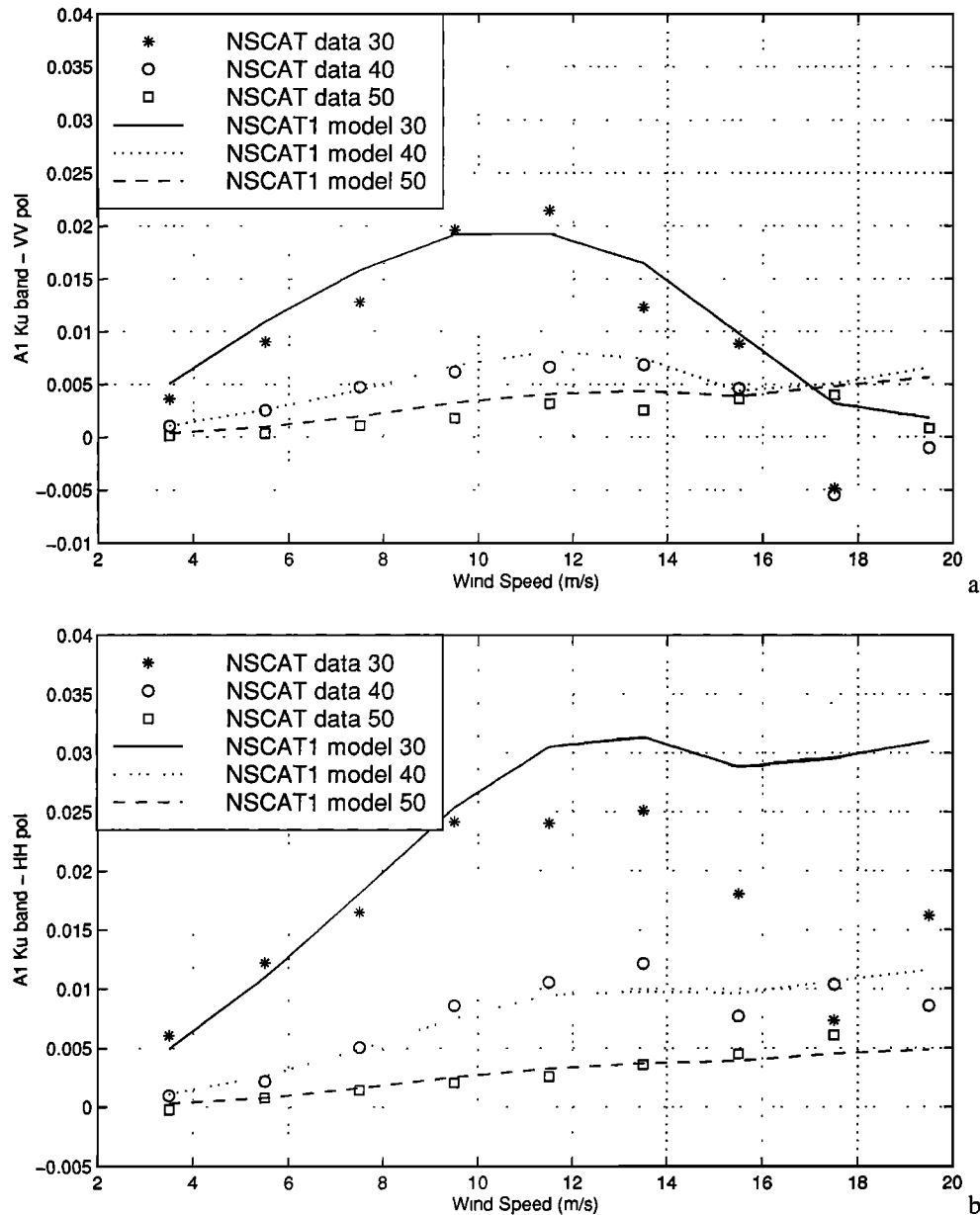


Figure 2. Estimates of a_1 at Ku band at (a) VV polarization and (b) HH polarization (lines), as computed from the measurements (symbols) and as derived from the NASA scatterometer (NSCAT 1) model (lines). Estimates are given as a function of wind speed for three different incidence angles.

the modeling of upwind/downwind a_1/a_0 ratio is not well suited and conflicts with the observed nonuniformity of a_1/a_0 behavior as a function of wind speed. For reasons related to the operational nature of the model, a_1/a_0 has been simply defined as a linear function of the wind speed. Thus the apparent differences between curves in Figure 1 were expected. These are reasonable and are due to the fact that CMOD-IFR2 optimizes (1) for best performance of the dominant terms a_0 and a_2 . This comparison indicates that model estimates and observations are still in very good agreement for wind speeds less than 14 m s^{-1} . For the highest wind speeds, systematic overestimations are predicted by the CMOD-IFR2 model function.

Figure 2 presents the equivalent analysis for global NSCAT measurements of Ku band VV and HH polarization (pol) a_1

parameters and for the NSCAT 1 empirical model jointly developed by M. H. Freilich and F. J. Wentz [Wentz and Smith, this issue]. Model and data both show magnitudes of NSCAT a_1 estimates are greater than for the ERS instrument at moderate wind speed and slightly lower at the highest winds. As for the ERS C band measurements, NSCAT a_1 coefficients for both polarizations first increase with wind speed and then decrease for the incident angles considered. The apparent saturation observed at C band is also confirmed in NSCAT data. In fact, it is more significant and occurs at a lower wind speed. At the 30° incidence angle, a_1 parameters for both polarizations seem to be somewhat enhanced at the lighter wind speeds. Also note that for VV polarization, an abrupt change is observed after 12 m s^{-1} , with a_1 actually taking on negative values above 16 m s^{-1} .

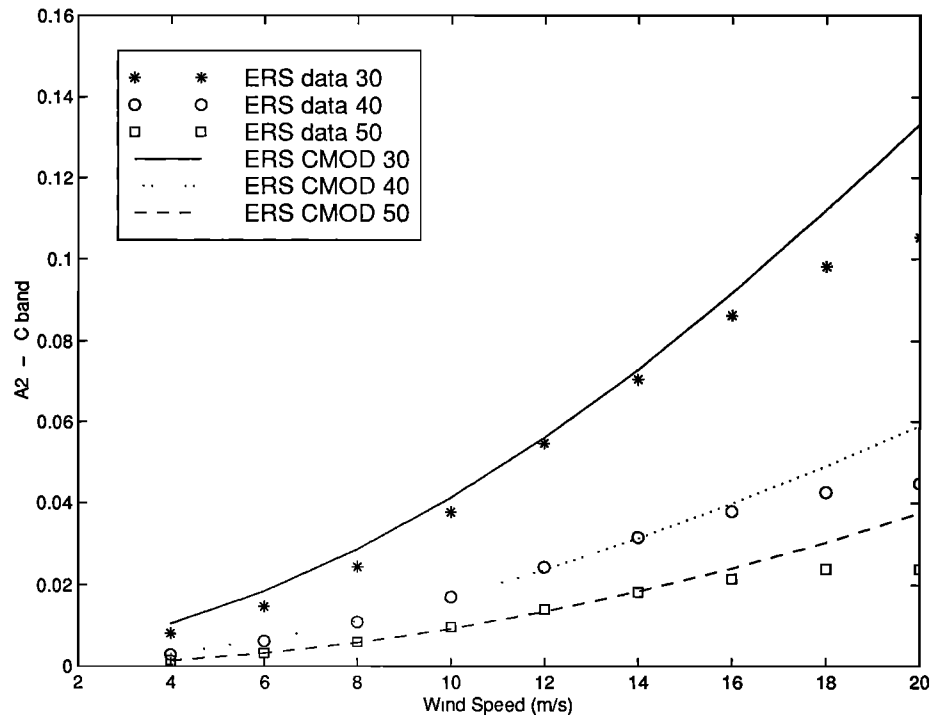


Figure 3. Estimates of a_2 at C band as computed from the measurements (symbols) and as derived from the CMOD-IFR2 model (lines) as a function of wind speed for three different incidence angles.

VV and HH pol estimates of Figure 2 are in close agreement in magnitude, HH results being slightly higher than VV, on average. Accepting that ocean surface radar cross sections are nominally much lower for HH than for VV configurations, such a result confirms previous experimental evidence [e.g., Masuko *et al.*, 1986; Long *et al.*, 1996] that upwind/downwind contrasts are significantly higher for HH pol than for VV pol. The comparison shown in Figure 2 indicates that NSCAT 1 estimates and observations are in very good agreement for wind speeds less than 16 m s^{-1} . For the highest wind speeds the NSCAT 1 model does not reproduce the negative a_1 values.

3.2. UCA Analysis

We conducted the same analysis for the a_2 parameter. Figure 3 shows the results for C band measurements and the CMOD-IFR2 model. As for a_1 , the a_2 coefficients are increasing with wind speed and decreasing with incidence angle. Although less pronounced, a_2 data also exhibit a saturation at the highest wind speeds. This comparison also revealed that C band model estimates and observations are generally in good agreement for wind speeds up to 15 m s^{-1} . However, a_2 model predictions are systematically overestimated for the lighter wind speeds at 30° incidence angle.

Figure 4 shows results from NSCAT data and the NSCAT 1 model. Similar trends are obtained and, as observed for ERS measurements, indicate a rapid increase for wind speeds above 5 m s^{-1} and an apparent slight saturation at higher wind speeds. Magnitudes of a_2 estimates are comparable between NSCAT and ERS instruments.

Note that while a_1 coefficients were not significantly different between HH and VV pol measurements, it is clear from this analysis that a_2 parameters are systematically lower for the HH than the VV configuration; the azimuthal modulation is

more pronounced for VV pol than for HH pol. This comparison also revealed that Ku band model estimates and observations are in very good agreement over the analyzed wind speed range, especially at VV polarization.

To better illustrate such properties and also to directly compare C and Ku band UCAs, we present results for the depth of azimuthal modulation parameter as defined by

$$\delta = \frac{a_0 + a_2}{a_0 - a_2} - 1 \quad (5)$$

Figure 5 gives δ as function of wind speed for the given incidence angle 45° and for both the measurements and empirical models. As obtained, VV pol C and Ku band results are comparable in shape and magnitude; a rapid increase is clearly noticeable for light to moderate wind speeds followed by a decrease at higher wind speeds. One clear difference is that the ERS C band VV pol depth of azimuthal modulation is reaching a maximum at about 12 m s^{-1} , while for NSCAT Ku band VV pol the maximum is at about $7\text{--}8 \text{ m s}^{-1}$.

Such behavior is not observed for HH pol data, where this depth of azimuthal modulation seems to remain constant with wind speed in contrast with VV configurations. No apparent maximum is observed. Such a large discrepancy between polarization states cannot be reproduced by a standard composite scattering model. Indeed, as defined by (5) and according to pure Bragg theory, δ computed at 45° incidence angle should only depend upon the shortwave surface spectral spreading function, $\delta_{\text{VV}} = \delta_{\text{HH}}$. This is clearly not the case for NSCAT Ku band data. Such a pronounced VV versus HH pol sensitivity difference must then be related to the fact that a pure Bragg-predicted HH pol cross section is systematically much lower than measurements. The comparison between δ measurements and NSCAT 1 model estimates indicates that the

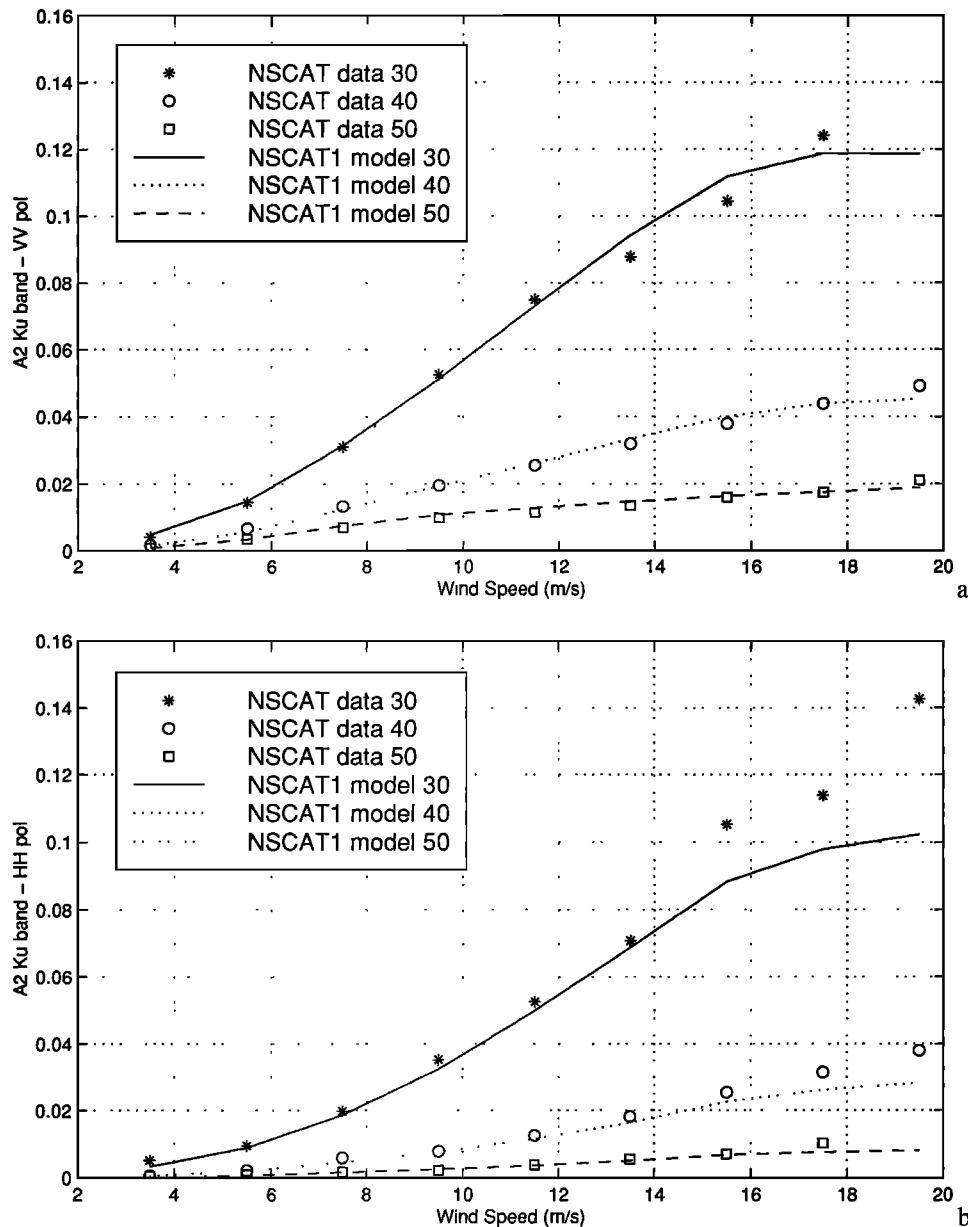


Figure 4. Estimates of a_2 at Ku band at (a) VV polarization and (b) HH polarization (lines), as computed from the measurements (symbols) and as derived from the NSCAT 1 model (lines). Estimates are given as a function of wind speed for three different incidence angles.

Ku band model δ are overestimated for the different analyzed incidence angles.

Overall, comparisons between measurements and empirical backscattering models, shown in Figures 1 to 5, indicate generally good agreement for the analyzed parameters as a function of the wind speed. Therefore, for clarity, in the following sections we use only the empirical model predictions to depict UCA and UDA behavior versus wind speed.

3.3. Heuristic Analysis of Upwind/Crosswind Observations

Model development for electromagnetic scattering from a random rough surface is an active topic, and a number of techniques and asymptotic theories exist. As mentioned earlier, most ocean scattering models for the scatterometer incidence angles have relied on the Bragg or composite surface

assumption. On the basis of the preceding presentation of NSCAT data, observed UCA differences between HH and VV pol will be difficult to reproduce with such a model. This supports the well-known finding that Bragg scattering theory may work well in describing VV-polarized ocean returns but that HH-polarized prediction will subsequently not match observations. For smaller incidence angles ($\leq 30^\circ$), a specular scattering component can be included within composite cross-section models that will improve predictions; but for larger incidence angles it is more difficult to involve the role of the longer waves. In this case, more sophisticated models have been developed through second-order inclusion of longer wave tilt combined with hydrodynamic modulations at short-scale Bragg components. It is often suggested that wedges and breaking waves, as well as multiple scattering phenomena

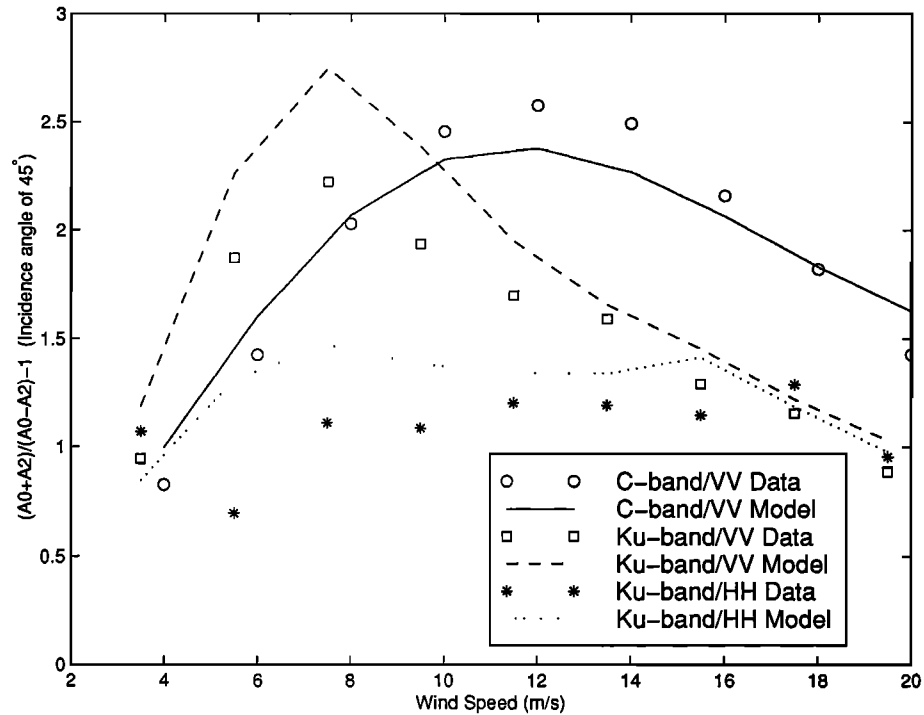


Figure 5. Depth of azimuthal modulation δ estimated from the measurements and from the empirical models at C band (circles, solid line), at Ku band VV polarization (squares, dashed line), and at Ku band HH polarization (stars, dotted line), as a function of wind speed for an incidence angle of 45° .

should be included; these latter contributions would then somewhat enhance HH-modeled predictions [e.g., Wetzel, 1990]. Recently, Plant [1997] also proposed the addition of small-scale bound waves to the standard composite surface model.

Proceeding from NSCAT data observations, we take an approach designed to isolate that scattering component associated with UCA. Assume that for this purpose Ku band radar backscatter returns at higher incidence angles can be well separated into two contributions, one of pure Bragg scattering type and one a non-Bragg scattering component, possibly associated with cusping and steep slopes. In such a model the latter contribution will be polarization state independent. We then express the total cross section as the sum of a scalar term and a polarization dependent term.

$$\sigma_{pp} = \sigma_{sc} + \sigma_{pol}^{pp} \quad (6)$$

With respect to the definition of the geometric functions that map shortwave spectral energy into backscatter for a Bragg model, the proposed assumptions lead to an HH-pol-dependent term that is much smaller at large incidence angles than the VV pol term. The nominal ratio is 1/9 for a perfectly conducting surface at 45° incidence angle. In such a way,

$$\sigma_{vv} - \sigma_{hh} \approx \sigma_{pol}^{vv} \quad \theta > 35^\circ \quad (7)$$

As verified in Figure 6a, the depth of azimuthal modulation defined from (5) and using (7) and over the range of incidence angle shown is found to have similar shape with larger maximum values compared with the results shown in Figure 5. It is then further found that the δ parameters are weakly incident angle dependent over the whole range of wind speed. Following such a development, δ observations are enhanced with a

rapid increase for light wind and a slower decrease after $7\text{--}8 \text{ m s}^{-1}$ wind speed.

Such a result may be compared with Figure 6b; δ parameters for different incidence angles are shown for C band VV-polarized measurements. It must be noted that the ratio between VV and HH has experimentally been found to be higher for a C band instrument than for a Ku band instrument [e.g., Unal et al., 1991]. Consequently, Bragg theory may be better adapted to describe C band radar returns. This would imply that the C band VV pol δ parameter should be even more directly related to the spectral spreading function of the short gravity-capillarity waves. From Figure 6 it can then be postulated that the maximum values for the depth of modulation are Bragg wavenumber dependent; the shorter Ku band Bragg scales, about 1.5 cm, aligned more rapidly with wind speed than the C band Bragg scales of about 3.5 cm. Under this interpretation the observations suggest the shorter surface waves adjust more quickly to wind direction but will appear omnidirectional as wind speed increases. The curves of Figure 6b show a particularly clear sensitivity to such an UCA change with shifting Bragg wavenumber.

Such a result must be related to the increasing influence of the surface drift current q on shortwave dissipation. The known effect is to limit the amplitude of the short gravity wavelets [Banner and Phillips, 1974]. This effect is stronger for wave components traveling in the direction of the wind speed. As a direct consequence, the growth of small-scale waves is limited in the direction of the wind, and their directivity in terms of δ strength should be lowered. More precisely, short waves of a given scale are expected to reach their maximum amplitude at stagnation points along the longwave profile. If c is the phase speed of the shortwave component, such a kine-

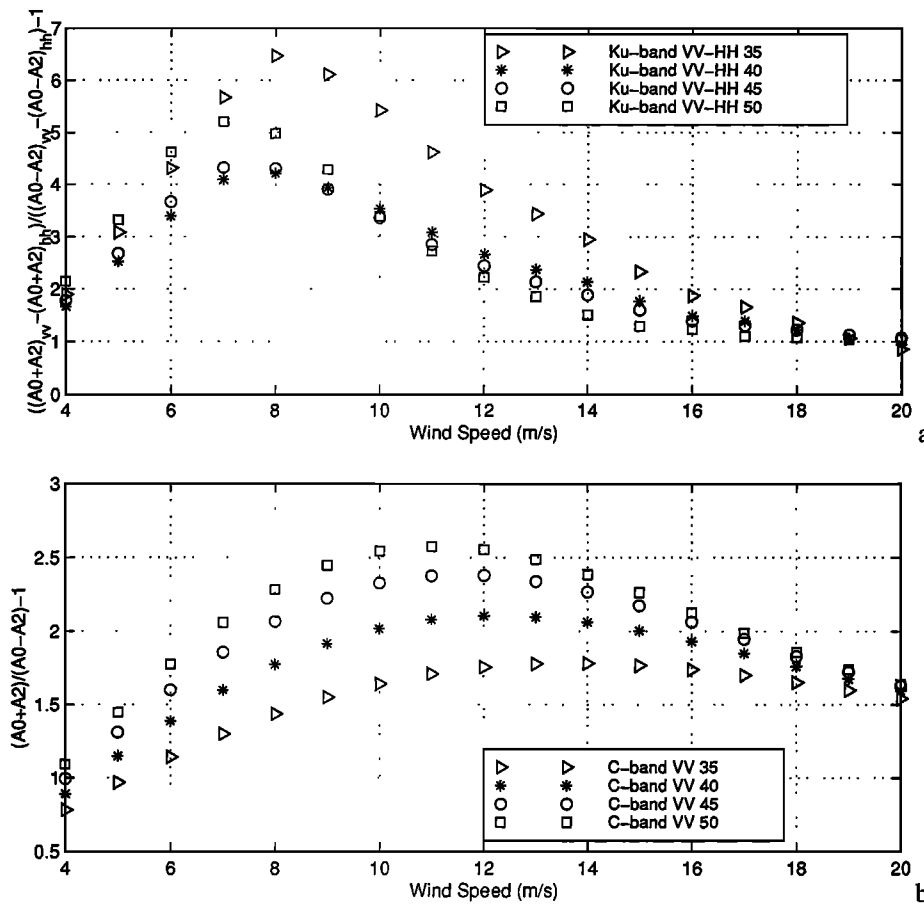


Figure 6. Depth of azimuthal modulation δ estimated from the empirical models as (a) Ku band from the VV–HH difference and (b) C band, as a function of wind speed for different incidence angles.

matic criterion can be written as $c \approx q_{\max}$, with q_{\max} being the surface drift augmented by long waves. To first order [e.g., Liu and Yan, 1995], q_{\max} may be simply linearly related to the amplitude of the orbital velocity u_0 , which in turn may also be approximated to be proportional to the mean wind speed U . In order to respect an equilibrium condition, a small mean wind speed variation will then be accompanied by a slight phase speed modification, such that $\partial c \propto \partial u_0 \propto \partial U$. Under such an assumption the maximum growth in the wind direction is expected to occur for a longer wave component as the wind speed increases. Figure 6b seems to confirm such a conclusion, the maximum δ value being shifted toward increasing wind speed when considering longer Bragg wave components (smaller incidence angles).

Reported in terms of the Bragg wave component phase speed at which the maximum δ value is obtained versus the corresponding wind speed, Figure 7 shows results combining VV–HH Ku band measurements and VV C band ones. The phase speed is obtained after deriving the Bragg wavenumber corresponding to the particular incidence angle and by using the standard dispersion relationship for capillary-gravity scales. C band maximum δ values have been obtained from 35° to 55° incidence angles. Ku band maximum δ values have been obtained from 35° to 50° incidence angles, no HH pol measurements being available at 55° incidence angle. Following a spectrum like that of the Joint North Sea Wave Project (JONSWAP) [Elfouhaily et al., 1997], the rms orbital velocity

may be directly related to wind speed as $u_0 = 0.06 U$. A recommended proportionality constant between q_{\max} and u_0 is 0.15 for open ocean conditions. As reported in Figure 7, the relationship $\partial c \approx 0.011 \partial U$ is consistent with the measurements, which indicates that the radar δ_{\max} signatures are well correlated with the expected short Bragg wave component behaviors. Acknowledging that q_{\max} is sea state dependent, results may indicate that the δ parameter will also be dependent on the sea state’s degree of development; for younger wind seas the corresponding critical phase speed will be higher, shifting the δ_{\max} value and leaving a smaller δ value for the given wind speed.

3.4. Skewness Analysis

Section 2 mentioned several methods for modeling observed scatterometer upwind/downwind data. Hereafter, we propose a differing illustration relying on the relationship between expected but unresolved skewness in the surface slope pdf and the slope tilt component in composite scattering models. Our objective is to introduce a simple conceptual model for UDA using skewness-induced tilting to modulate the radar cross section.

A description of the random sea surface that includes weak nonlinearity has been depicted by Longuet-Higgins [1963, 1982]. His approach in assigning non-Gaussian properties to the ocean surface wave slope pdf relies, in part, on the measurement and analysis of sea surface slope statistics as given by

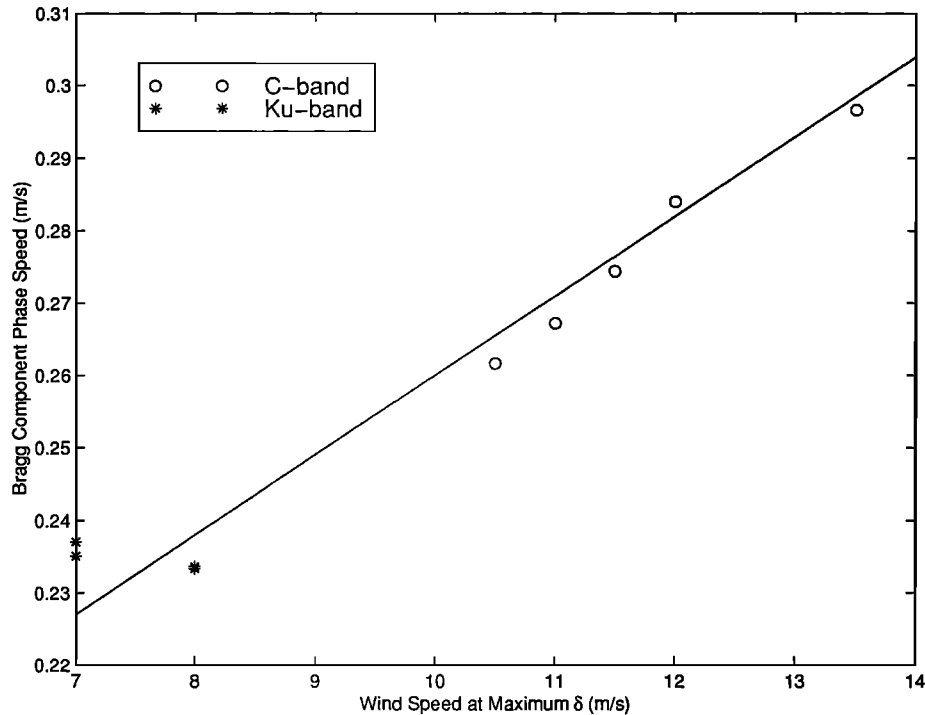


Figure 7. Inferred phase speed of the Bragg waves at C band (circles), Ku band (stars), and as derived from the estimated incipient breaking criterion (solid line), for which the depth of azimuthal modulation (see Figure 6) is maximum. Estimates are presented as a function of wind speed. The phase speed is calculated for incidence angles from 35° to 55° at C band and from 35° to 50° at Ku band. Note that two NSCAT points nearly overlap.

Cox and Munk [1954]. To describe the deviations from a Gaussian surface slope distribution, a more generalized Gaussian distribution was proposed using a Gram-Charlier expansion. Truncated to its third order, this distribution will depend upon the definition of skewness parameters.

A simple geometrical result of the existence of skewness is an angular shift of the slope pdf away from the origin. The distribution remains nearly Gaussian, but there is a small “pointing angle” shift Δ [e.g., *Longuet-Higgins*, 1982, Figure 1] toward the downwind direction. Note that no skewness was measured or modeled in the crosswind direction.

As a first application of non-Gaussian slope pdf to scatterometry, we suggest a simple empirical link based on the following association. Slope statistics represent information related to short-scale wave structure; wave slope is primarily carried across wavenumbers between about 20 and 700 rad m^{-1} . Therefore, while the third-order slope statistic is not explicitly ascribed to a particular band within the short-scale wave regime, nonetheless, the phenomenon is carried within the total slope pdf. The radar’s backscatter, including UDA, is predominantly from these same short-scale waves. So while it may be untenable to specify explicit skewness in a surface description input to a scattering model, the anisotropy of the optical and radar measurements may still be empirically linked to aid investigations.

Now, regardless of a chosen scattering theory, the angular deviation Δ can be interpreted as introducing a small pointing angle perturbation causing an upwind/downwind modulation of σ_0 . Since scatterometer backscattered power is a decreasing function with incidence angle, we can hypothesize that for

small positive Δ , radar returns will be higher looking upwind than looking downwind.

Scatterometer UDA measurements at a particular incidence angle can be used to derive an empirical, “effective” shift angle Δ_{eff} . In the weakly decreasing σ_0 incidence angle region, i.e., $40^\circ \leq \theta \leq 60^\circ$, assume that the upwind/downwind term a_1 is small (a good approximation, as nominally $a_1 < a_2 < a_0$). Under a small perturbation approximation we can define the shift angle as

$$\Delta_{\text{eff}} \approx -a_1 \left[\frac{\partial(a_0 + a_2)}{\partial \theta} \right]^{-1} \quad (8)$$

Figure 8 shows results of (8) for C and Ku band global measurements. As expected from earlier data analysis, Δ_{eff} is found to be larger for HH than for VV Ku band measurements. For C band, Δ_{eff} is a continuously increasing function of the wind speed. For Ku band, Δ_{eff} is a decreasing function for wind speed higher than 10 m s^{-1} .

As already mentioned, slope skewness measurements have been reported from optical Sun glitter measurements by *Cox and Munk* [1954]. Their measurements clearly show that under slick surface conditions, Δ is negligible. They also reported that Δ increases with wind speed in their range of wind conditions, i.e., $U_{10} \leq 14 \text{ m s}^{-1}$. Thus when compared to our global radar analysis, optical measurements appear to be more consistent with C band measurements than with Ku band. As noted in section 3.1, the discrepancy between the C band model a_1 and the data does not allow one to draw any conclusion for winds greater than 14 m s^{-1} .

The combination of these findings appears to provide insight

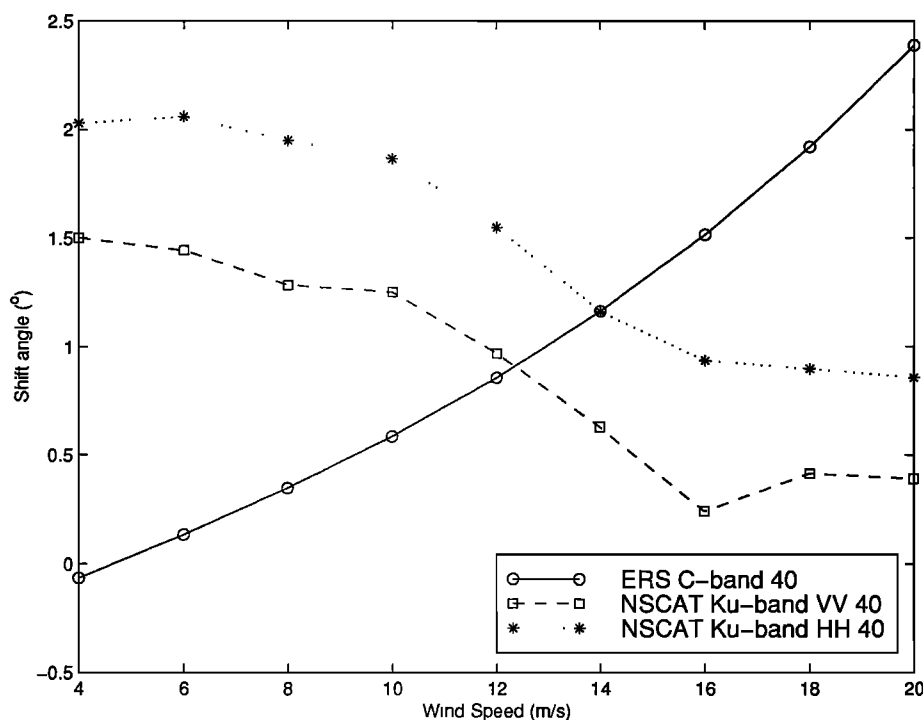


Figure 8. Shift angle (Δ_{eff}) estimated from the empirical models at C band (circles, solid line), at Ku band VV polarization (squares, dashed line), and at Ku band HH polarization (stars, dotted line), as a function of wind speed and for an incidence angle of 40° .

into the region(s) of the spectrum supporting the skewness. Our preliminary interpretation is that the slope skewness is supported by short gravity waves rather than the waves in the capillary-gravity region.

4. Conclusion

In this paper, UCA and UDA characteristics have been derived from C band VV polarized ERS 1 and 2 and Ku band VV- and HH-polarized NSCAT data. As revealed from the analysis of large global data sets, the VV-polarized radar signature for both instruments can be considered to be consistent with a Bragg scattering mechanism from capillary-gravity waves. However, pure Bragg theory may be better adapted to describe C band returns.

To better illustrate UDA and UCA properties, we introduce the use of two conceptual tools: the depth of azimuthal modulation δ , equation (5), and the effective shift angle Δ_{eff} , equation (8). The latter parameter has been chosen to help comparisons between observed radar UDA and optically derived slope skewness measurements. Our results show that Δ_{eff} parameters are quite different for C or Ku band data, the results for C band being more consistent with *Cox and Munk's* [1954] Sun glitter observations. Our preliminary interpretation is that the C band may be easier to interpret using composite Bragg scattering theory and that the slope skewness is mainly supported by short gravity waves.

Using the δ parameter, it has been clearly identified that UCA is not monotonically increasing with wind speed. Following the Bragg assumption, it has been further shown that surface drift effects may be of fundamental importance in understanding the observed saturation. As postulated, the short surface wave component growth in the wind direction is limited

owing to wave-drift interactions. The observations suggest the shorter surface waves as probed by a Ku band instrument adjust more quickly to wind direction but become saturated in the wind direction as wind speed increases. Using global data sets, the average wind speed at which the δ parameter is maximum is found to be consistent with an averaged small-scale wave incipient breaking criterion. The sea state degree of development being known to directly affect surface wind drift modulations, it should also influence UCA radar signatures. In the future, investigations will be conducted to identify geographical differences in δ UCA and Δ_{eff} UDA parameters in terms of sea state parameters.

For operational purposes the greater UCA and UDA measurements at Ku band compared C band for moderate to light winds suggest better retrieval of the wind direction at Ku band in that wind speed range. On the other hand, as outlined by *Long et al.* [1996], greater Ku band geophysical variability (environmental parameters plus atmospheric attenuation) could suggest the opposite conclusion. Simulations of the wind retrieval process together with a careful analysis of the operationally retrieved winds may determine whether one frequency is better adapted.

References

- Banner, M. L., and O. M. Phillips, On the incipient breaking of small scale waves, *J. Fluid Mech.*, 4, 647–656, 1974.
- Bentamy, A., Y. Quilfen, P. Queffeuou, and A. Cavanié, Calibration and validation of ERS-1 scatterometer, *Tech. Rep. DRO-OS-94-01*, 72 pp., Inst. Fr. Rech. pour l'Exploit. de la Mer, Brest, France, 1994.
- Caudal, G., and D. Hauser, Directional spreading function of the sea wave spectrum at short scale, inferred from multifrequency radar observations, *J. Geophys. Res.*, 101, 16,601–16,613, 1996.
- Chen, K. S., A. K. Fung, and D. E. Weissman, A backscattering model

- for ocean surface, *IEEE Trans. Geosci. Remote Sens.*, *30*, 811–817, 1992.
- Chen, K. S., A. K. Fung, and A. Faouzi, An empirical bispectrum model for ocean surface, *IEEE Trans. Geosci. Remote Sens.*, *31*, 830–835, 1993.
- Cox, C. S., and W. H. Munk, Measurements of the roughness of the sea surface from photographs of the sun's glitter, *J. Opt. Soc. Am.*, *44*, 838–850, 1954.
- Elfouhaily T., B. Chapron, K. Katsaros, and D. Vandemark, A unified directional spectrum for long and short wind-driven waves, *J. Geophys. Res.*, *102*, 15,781–15,796, 1997.
- Freilich, M. H., and R. S. Dunbar, A preliminary C-band scatterometer model function for the ERS-1 AMI instrument, in *Proceedings of First ERS-1 Symposium: Space at the Service of Our Environment*, Eur. Space Agency Spec. Publ., ESA SP-359, 79–83, 1993.
- Fung, A. K., *Microwave Scattering and Emission Models and Their Applications*, Artech House, Norwood, Mass., 1994.
- Jet Propulsion Laboratory (JPL), Science data product user's manual, *Tech. Rep. D-12995*, Pasadena, Calif., 1997.
- Liu, Y., and X.-H. Yan, The wind-induced wave growth rate and the spectrum of the gravity-capillary waves, *J. Phys. Oceanogr.*, *25*, 3196–3218, 1995.
- Long, F. J., R. S. Collyer, R. Reed, and D. V. Arnold, Dependence of the normalized radar cross section of water waves on Bragg wavelength-wind speed sensitivity, *IEEE Trans. Geosci. Remote Sens.*, *34*, 656–666, 1996.
- Longuet-Higgins, M. S., The effects of non-linearities on statistical distribution in the theory of sea waves, *J. Fluid Mech.*, *17*, 459–480, 1963.
- Longuet-Higgins, M. S., On the skewness of sea-surface slopes, *J. Phys. Oceanogr.*, *12*, 1283–1291, 1982.
- Masuko, H., K. Okamoto, M. Shimada, and S. Niwa, Measurement of microwave backscattering signatures of the surface using X-band and Ka-band airborne scatterometers, *J. Geophys. Res.*, *91*, 13,065–13,083, 1986.
- Plant, W. J., A two-scale model of short wind-generated waves and scatterometry, *J. Geophys. Res.*, *91*, 10,735–10,749, 1986.
- Plant, W. J., A model for microwave Doppler sea return at high incidence angles: Bragg scattering from bound, tilted waves, *J. Geophys. Res.*, *102*, 21,131–21,146, 1997.
- Quilfen, Y., and A. Bentamy, Calibration/validation of ERS-1 scatterometer precision products, in *Proceedings of IGARSS'94*, pp. 945–947, IEEE Press, Piscataway, N. J., 1994.
- Quilfen, Y., B. Chapron, T. Elfouhaily, K. Katsaros, and J. Tournadre, Observation of tropical cyclones by high-resolution scatterometry, *J. Geophys. Res.*, *103*, 7767–7786, 1998.
- Romeiser, R., and W. Alpers, An improved composite surface model for the radar backscattering cross section of the ocean surface: Model response to surface roughness variations and the radar imagery of underwater bottom topography, *J. Geophys. Res.*, *102*, 25,251–25,267, 1997.
- Schroeder, L. C., D. H. Boggs, G. Dome, I. M. Halberstam, W. L. Jones, W. J. Pierson, and F. J. Wentz, The relationship between wind vector and normalized radar cross section used to derive SeaSat-A satellite scatterometer winds, *J. Geophys. Res.*, *87*, 3318–3336, 1982.
- Stoffelen, A., Error modeling and calibration: Toward the true surface wind speed, *J. Geophys. Res.*, *103*, 7755–7766, 1998.
- Stoffelen, A., and D. Anderson, Scatterometer data interpretation: Estimation and validation of the transfer function CMOD4, *J. Geophys. Res.*, *102*, 5767–5780, 1997.
- Unal, C. M. H., P. Snoeij, and P. J. F. Swart, The polarization-dependent relation between radar backscatter from the ocean surface and surface wind vector at frequencies between 1 and 18 GHz, *IEEE Trans. Geosci. Remote Sens.*, *29*, 621–626, 1991.
- Wentz, F. J., and D. K. Smith, A model function for ocean-normalized radar cross section at 14 GHz derived from NSCAT observations, *J. Geophys. Res.*, this issue.
- Wetzel, L. B., Electromagnetic scattering from the sea at low grazing angles, in *Surface Waves and Fluxes*, vol. 2, edited by G. Geernaert and W. J. Plant, pp. 109–171, Kluwer Acad., Norwell, Mass., 1990.
- Wu, J., Mean square slopes of the wind-disturbed water surface, their magnitude, directionality, and composition, *Radio Sci.*, *25*, 37–48, 1990.
- A. Bentamy, B. Chapron, J. Gourrion, and Y. Quilfen, Département d'Océanographie Spatiale, IFREMER, BP 70, 29280 Plouzané, France (yquilfen@ifremer.fr).
- T. El Fouhaily and D. Vandemark, NASA Goddard Space Flight Center, Wallops Flight Facility, Laboratory for Hydrospheric Processes, Wallops Island, VA 23337.

(Received February 23, 1998; revised November 30, 1998; accepted December 9, 1998.)